Landslides triggered by the 2015 Mw 6.0 Sabah (Malaysia) earthquake: inventory and ESI-07 intensity assignment

Maria Francesca Ferrario[1]

[1] Università dell'Insubria, Dipartimento di Scienza e Alta Tecnologia, Como 22100, Italy

Correspondence to: M. F. Ferrario (francesca.ferrario@uninsubria.it)

Abstract. On 4 June 2015, a Mw 6.0 earthquake occurred in the Sabah region (Malaysia), triggering widespread landslides
along the slopes of Mt. Kinabalu. Despite the moderate magnitude, the Sabah earthquake was very efficient in triggering
landslides: here I provide an inventory containing 5198 slope movements, mapped in an 810 km^2-wide area. I investigate
earthquake intensity using the Environmental Seismic Intensity (ESI-07) scale, which is a macroseismic scale based
exclusively on earthquake environmental effects. The epicentral ESI-07 intensity is assessed at IX, considering the
dimension of the area affected by secondary effects; such figure agrees well with a dataset of global earthquakes.
I estimate the volume of individual landslides using area-volume scaling laws, then I assigned an ESI-07 intensity to each
mapped landslide. I document that the selection of a given area-volume relation has a minor influence on the ESI-07
assignment. Then, I compare ESI-07 values to landslide density and areal percentage on a 1-km^2 grid; such parameters are
widely adopted in the description of earthquake-triggered landslide inventories. I argue that their integration with the ESI-07
scale may provide an effective way to compare earthquake damage on a variety of spatial and temporal scales. The
methodological workflow here illustrated is useful in joining the scientific communities dealing with the realization of
earthquake-triggered landslide inventories and with ESI-07 assignment; I believe this effort is beneficial for both the
communities.

1 Introduction

Moderate to strong earthquakes cause widespread damage due to primary effects, (i.e., those related to the seismogenic
source) or due to ground shaking. Earthquakes often initiate a cascade of effects, which bring different degrees of hazard and
worsen the overall damage (Williams et al., 2018; Fan et al., 2019; Quigley et al., 2020). The frequency and impact of
disasters is increasing in the last years and this trend is not expected to change in the future; additionally, modern societies
are vulnerable due to the complex interdependencies existing among the territory and infrastructure systems (Harrison &
Williams, 2016). Cascading events are function of time and space and follow non-linear paths. When hitting critical nodes,
they lead to enhanced direct and indirect losses: thus, assessing systemic interdependencies and including cascading effects
into simulation tools is crucial for pursuing a more comprehensive knowledge and supporting preparedness, mitigation and
recovery measures (Pescaroli & Alexander, 2016; Zuccaro et al., 2018).

Earthquake damage is usually assessed by means of macroseismic intensity, i.e., a classification of effects on humans, the
built and the natural environment (Cecić and Musson, 2004). Among the different intensity scales, the Environmental
Seismic Intensity (ESI-07) is the only one based exclusively on environmental effects (Michetti et al., 2004, 2007; Serva et
al., 2016; Ferrario et al., 2022). Landslides are one of such environmental effects and may be a significant cause of damage
and casualties (Marano et al., 2010; Budimir et al., 2014). Inventories of landslides triggered by earthquakes are crucial for
hazard analyses and land planning (Keefer, 1984; Harp et al., 2011; Xu, 2015); currently tens of inventories are available for
a variety of territorial and climatic settings (Schmitt et al., 2017; Tanyas et al., 2017). Landslide inventories were usually

2

derived from manual mapping on aerial or satellite images, but in the last years several efforts have been undertaken to automatically map earthquake-triggered landslides (e.g., Burrows et al., 2020; Handwerger et al., 2020); nevertheless, manually-derived inventories are needed to ascertain the validity and accuracy of (semi)-automatic methods. Landslide number, density and areal percentage vary in the affected area and are often analyzed with respect to topography, seismological or geological conditions (e.g., Chang et al., 2021; Fan et al., 2018; Ghaedi Vanani et al., 2021; Papathanassiou et al., 2021; Wang et al., 2019; Xu et al., 2014).

To date, the scientific communities dealing with the building of landslide inventories and with ESI-07 assignment have proceeded on parallel paths with limited mutual interactions. I believe that an enhanced cooperation may benefit each other: modern landslide inventories have a resolution higher than what is usually achieved by studies focused on the ESI-07 scale; on the other hand, the ESI-07 scale enables the comparison of earthquakes damage through time and space.

Here I analyze the Mw 6.0 Sabah (Malaysia) earthquake, occurred on 4 June 2015. First, I build an inventory comprising 5198 landslides; then, I calculate the landslide number density (LND), landslide area percentage (LAP) and ESI-07 intensity on a 1-km^2 grid. ESI-07 assignment requires to convert landslide area to volumes: thus, I explore the epistemic uncertainty associated to different scaling relations. I analyze the interdependency of LND, LAP and ESI-07; since it is expected to have a regional validity, the analysis of additional case histories is needed to assess the reliability of empirical regressions and their stability under different territorial settings. The methodological workflow presented here is aimed at strengthening the exchange of information between different scientific communities; outputs will be useful to inform advancements in ground failure models and for land planning and risk assessment.

2 Regional setting and the 2015 Sabah earthquake

2.1 Seismotectonic setting

Sabah region lies in a complex seismotectonic setting at the junction of Australian plate, Philippine plate and the Sundaland block. Sabah belongs to Malaysia and it is located in the northern part of Borneo Island. Seismicity is diffuse along the plate boundaries (Fig. 1a), where the subduction interface is located. Less frequent earthquakes have been recorded in the Ranau region, including a Mw 5.3 in 1966 and a Mw 5.2 in 1991. Offshore Sabah, the NW Borneo trench is a deep-water fold-and-thrust belt; its structural setting is debated and it has been related either to gravity sliding or to tectonic shortening (Hall, 2013; Sapin et al., 2013). GPS measurements show that, despite the absence of seismicity, the NW Borneo trench may accommodate up to 5 mm/yr (Simons et al., 2007). GPS data also assess that Sabah is actively deforming, albeit at a slower rate than the surroundings (Simons et al., 2007; Mustafar et al., 2017); this contradicts the earlier view of a rigid Sundaland block.
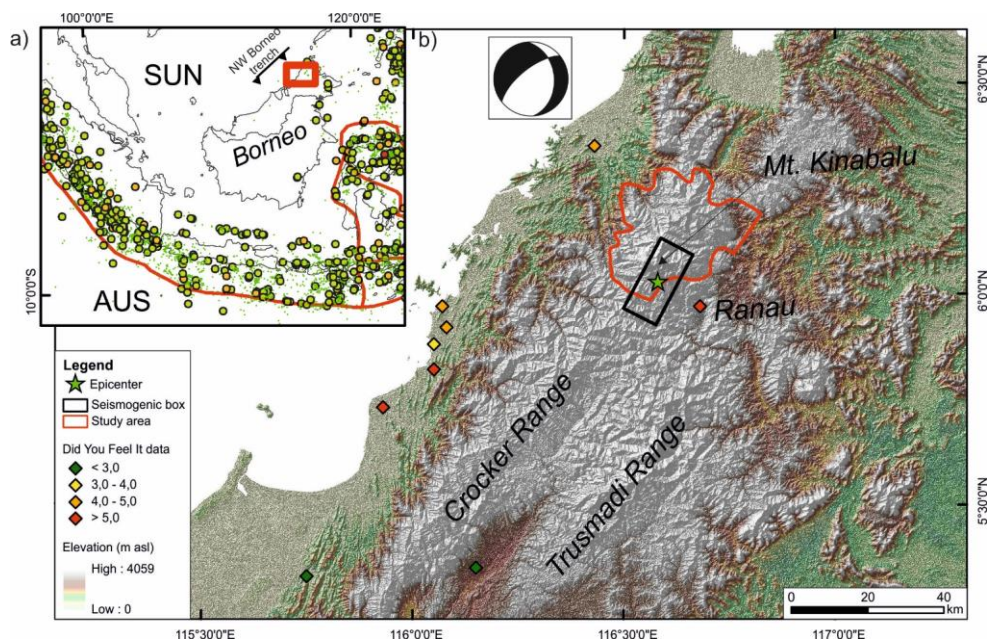
Figure 1: a) Regional seismotectonic setting of SE Asia showing main plate boundaries and M > 5 earthquakes (USGS/NEIC catalogue); AUS: Australian Plate, SUN: Sundaland block; the red rectangle marks the area enlarged in b. **b)** Digital elevation model derived from 30-m resolution ALOS DEM; focal mechanism is from USGS, epicenter and seismogenic box after Wang et al. (2017); intensity data from DYFI program are shown as well.

2.2 The study area and the 2015 Sabah earthquake

Sabah is characterized by rugged topography, dominated by the Crocker and Trusmadi Ranges; the highest peak is Mount Kinabalu, reaching 4100 m asl and representing the first World Heritage Site in Malaysia. It is a granitic pluton exposed over a ca. 120 km^2-wide area and it was exhumed about 7 My ago (Cottam et al., 2010). Beside the granitic pluton, Oligocene-Lower Miocene sandy turbidites constitutes the Crocker Formation, while the Trusmadi Formation comprises argillite, slate, siltstone and sandstone with volcanics (Hutchinson et al., 2000). Sabah is covered by thick tropical forests and the climate is characterized by monsoonal seasons (November to March and May to September); rainfall is high (> 3000 mm/yr) but highly variable due to local topography (Menier et al., 2017).
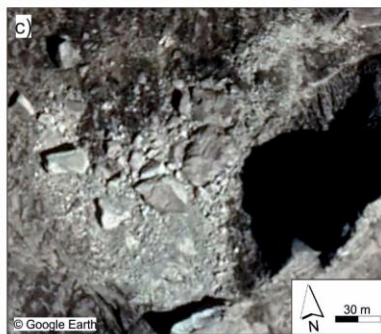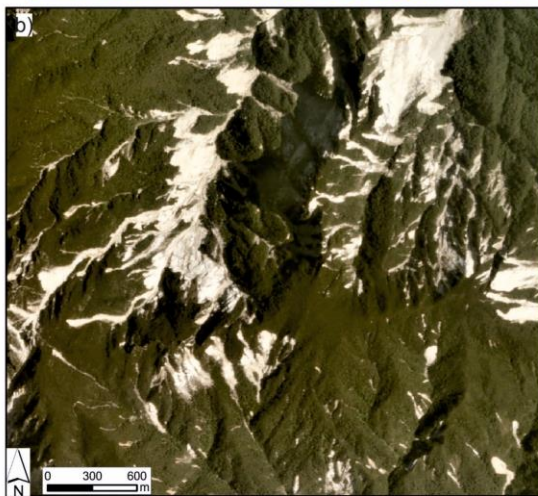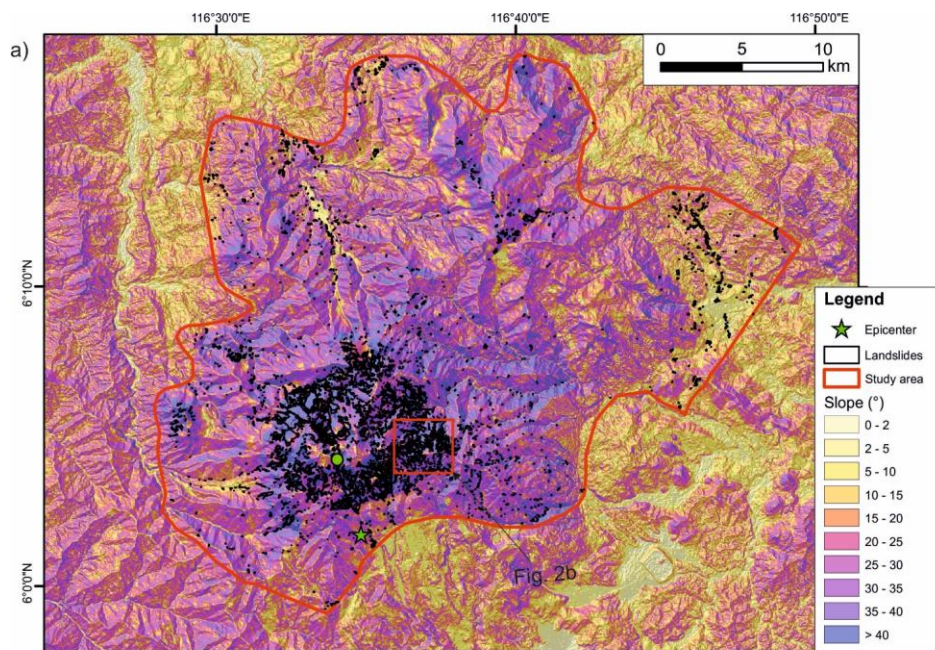
Several faults have been mapped in the region, mainly based on tectonic geomorphology and watershed analyses (e.g., Mathew et al., 2016; Menier et al., 2017; Shah et al., 2018). Sedimentary basins bounded by normal faults are indeed aligned

4

along the Crocker and Trusmadi Ranges; geomorphological features pointing to a recent tectonic activity include triangular facets, scarps and river anomalies (Tija, 2007; Tongkul, 2017; Wang et al., 2017). Laterally offset features (terraces, river courses) allow to identify strike-slip structures that crosses Borneo (Shah et al., 2018).

90 The Mw 6.0 Sabah earthquake occurred on 4 June 2015 at 23.15 UTC at 10 km depth (USGS, 2018); it is the largest instrumental event in the province. The event had a normal focal mechanism, with a NE-SW oriented main focal plane. The seismogenic box and relocated epicenter after Wang et al. (2017) are shown in Fig. 1b. The seismogenic source of the 2015 Sabah earthquake belongs to a system of normal faults of about 200 km length that lies at the foothills of the Crocker Range (Tjia, 2007; Tongkul, 2016, 2017; Wang et al., 2017).

95 "Did You Feel It?" data acquired by the USGS include sparse intensity estimations, with maximum values of 6.6 on the CDI (Community Decimal Intensity) scale at Ranau. The earthquake did not generate primary surface faulting and a directivity toward Mt. Kinabalu has been inferred based on teleseismic waveform inversion and space-based geodesy (Wang et al., 2017). The event generated thousands of landslides and rockfalls (Tongkul, 2017; Wang et al., 2017) which caused the death of 18 people along hiking routes on Mt. Kinabalu. Additionally, water infrastructures were damaged and local businesses

100 badly affected (Lehan et al., 2020).

The landslide deposits provided abundant sediments for subsequent remobilization as debris flows following heavy rainfall (highest rainfall intensity of 14.2 mm/h on 15 June 2015; Rosli et al., 2021a). Some detailed studies of debris flows were performed on limited areas through Lidar techniques (Yusoff et al., 2016; Rosli et al., 2021a, b), but a comprehensive inventory of all the triggered landslides is still lacking and is the focus of this paper.

a)

116°30'0"E   116°40'0"E   116°50'0"E

0   5   10
km

6°10'0"N

6°0'0"N

Fig. 2b

Legend

★ Epicenter

☐ Landslides

☐ Study area

Slope (°)

0 - 2
2 - 5
5 - 10
10 - 15
15 - 20
20 - 25
25 - 30
30 - 35
35 - 40
> 40

b)

0   300   600
m

N

c)

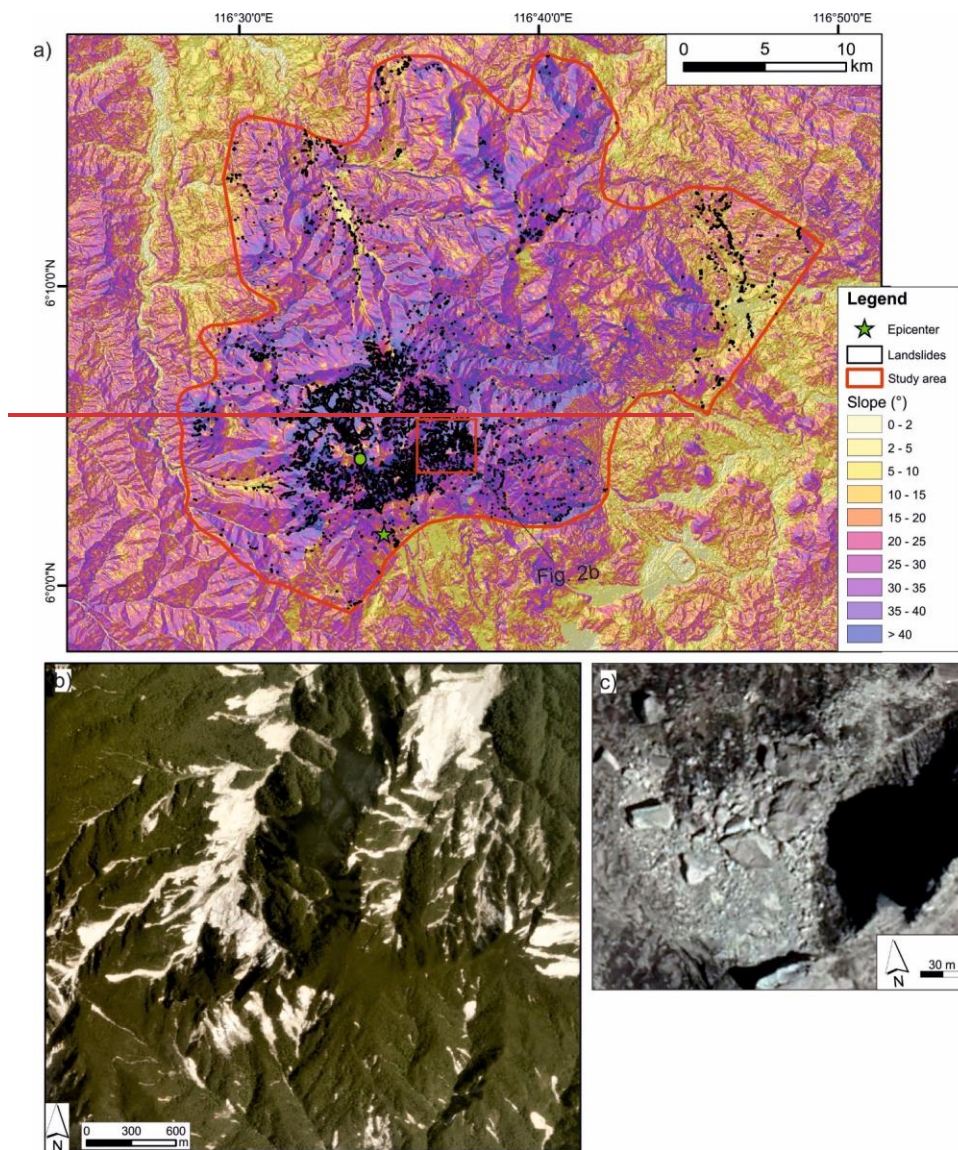© Google Earth

30 m

N

105

6

Figure 2: a) Slope map and hillshade derived from 30-m resolution ALOS DEM; the red polygon is the study area, while landslides are shown in black; b) Planet Labs image (3-m resolution) taken on 18 March 2016 showing widespread landslides; c) Google Earth image of a rockfall on top of Mt. Kinabalu (location is the green dot in Fig 2a).

110 **3 Materials and methods**

3.1 Landslide inventory

I realized a landslide inventory in an 810 km^2-wide area (red polygon in Fig. 2a) using ~~a~~ QGIS ~~platform~~software; the inventory is based on visual interpretation of 3-m resolution PlanetScope satellite images. I used high resolution Google Earth images to gain a regional overview, while individual landslides are mapped on ortho-rectified 4-band multispectral

115 tiles. The landslide inventory is realized on images taken on 23 February, 18 and 21 March 2016; such images postdate the earthquake by about 8 months and thus the inventory has to be intended as the cumulative damage due to the mainshock, aftershocks and additional remobilization (e.g., debris flows, Rosli et al., 2021a, b). This is a limitation that should be considered when comparing the obtained database with other case histories; it is due to persistent cloud cover that prevented the acquisition of clear images over the entire area closer in time to the mainshock. Cloud-free PlanetScope images are not

120 available for the time preceding the earthquake; preexisting landslides were thus identified from multi-temporal Google Earth historical images, acquired between May 2008 and April 2015.

Landslides were mapped as polygons encompassing the source and deposit areas. Shallow landslides were easily recognizable in forested regions, since they stripped off the vegetation (Fig. 2b). Mapping was more difficult in the higher part of Mt. Kinabalu pluton, since bare rock was already outcropping before the earthquake; in this sector, brighter colors on

125 post-event images was used as an indication of the occurrence of slope movements. Landslide mapping may suffer from problems related to amalgamation of coalescing polygons, i.e., the mapping of several adjacent landslides as a single polygon (Marc and Hovius, 2015)~~, which further bias the computation of landslide number.~~ This problem is especially severe for inventories realized through automatic mapping and may introduce a bias in the computation of landslide number and other statistics (e.g., ESI-07 assessment). When multiple sources areas coalesce in a single toe sector, it is difficult to

130 identify individual landslides. In such cases, I first mapped the entire polygon, then I used the "split" tool to delineate the different source areas. This GIS tool allows to draw contiguous polygons, avoiding the overlap of different polygons, or unmapped areas in between.

~~To avoid this problem, when multiple source areas coalesce in the lower sector, I used the "split" tool to divide polygons.~~

3.2 Landslide number density (LND), landslide areal percentage (LAP) and ESI-07 intensity assignment

135 The study area (Fig. 2a) was divided in a grid of 1 km x 1 km cells and the centroids of each landslide polygon were extracted. The LND is calculated as the sum of the centroids fitting in each 1 km x 1 km grid cell. LAP represents the percentage of the area covered by the mapped polygons within each cell. Additionally, I define "landslide area" as the sum

of areas of individual landslides, while I use "affected area" to indicate the region encompassing all the mapped slope movements.

140 ESI-07 intensity assignment requires to estimate volumes of each landslide. This can be achieved via field surveys, which however are not feasible for all the landslide population, or by differencing of high resolution pre- and post-landslide elevation models (e.g., Massey et al., 2020). When such data are not available, area-volume empirical relations are commonly used (Guzzetti et al., 2009; Fan et al., 2019); to assess the epistemic uncertainty related to the area-volume conversion, I tested multiple equations (Table 1), which have the general form:

145
$$V = \alpha \times A_i^{\gamma} \quad (1)$$

Where V is volume in m^3, A_i is the area of individual landslides in m^2, and α and γ are fitting coefficients.

Table 1: Area-volume scaling relations considered in this study.

Nr.	Equation	α	γ	Notes
1	Guzzetti et al., 2009	0.074	1.450	Global, slide type, several triggering processes
2	Larsen et al., 2010 (all)	0.146	1.332	Global, all types
3	Larsen et al., 2010 (bedrock)	0.186	1.350	Global, bedrock
4	Larsen et al., 2010 (soil)	0.257	1.145	Global, soil
5	Xu et al., 2016	1.315	1.208	Subset of landslides triggered by 2008 Wenchuan earthquake
6	~~Massey et al., 2020~~	~~0.891~~	~~1.109~~	~~Landslides triggered by 2016 Kaikoura earthquake; volume estimated from Lidar-derived data~~
6	Benjamin et al., 2018	0.588	1.202	Rockfalls on coastal cliffs at Staithes (UK); 2D change detection from Terrestrial Laser Scanner point clouds
7	Caputo et al., 2018	0.729	1.125	Rockfalls on coastal cliffs at Coroglio (Italy); volume estimated from Terrestrial Laser Scanner data

150
The ESI-07 guidelines (Michetti et al., 2004; 2007) include typical values of landslide volume for each intensity degree; thus, I used the volume derived with Equation (1) to assign an ESI-07 intensity to each landslide polygon, following the thresholds presented in Table 2. It must be noted that landslide dimension saturates at ESI-07 X (i.e., it is not possible to define degrees higher than X based on individual landslides). To compare ESI-07 to LND and LAP values, the highest ESI-
155 07 value is retained for each grid cell, adopting an approach similar to Ota et al. (2009) and Silva et al. (2013).

LND, LAP and ESI-07 focus on different aspects, as illustrated in Fig. 3. The three panels have the same LAP (36% of the "study region", i.e., the black square); the area of the biggest landslide is used to compute the ESI-07 value, as done for the

real case study. In this example, the Guzzetti et al. (2009) equation is used to illustrate the results. The first scenario (Fig. 3a) shows one wide landslide, resulting in an ESI-07 value ≥X. The second case shows 36 small landslides and is equivalent to

160   ESI-07 VIII. The third case shows the presence of one medium-sized and 30 small landslides, resulting in ESI-07 value of IX. Fig. 3 highlights that the concurrent evaluation of LND, LAP and ESI-07 provide an added value in the understanding of the distribution and characteristics of the landslide inventory, due to the role played by the number and dimension of individual landslides in the calculation of the different metrics.

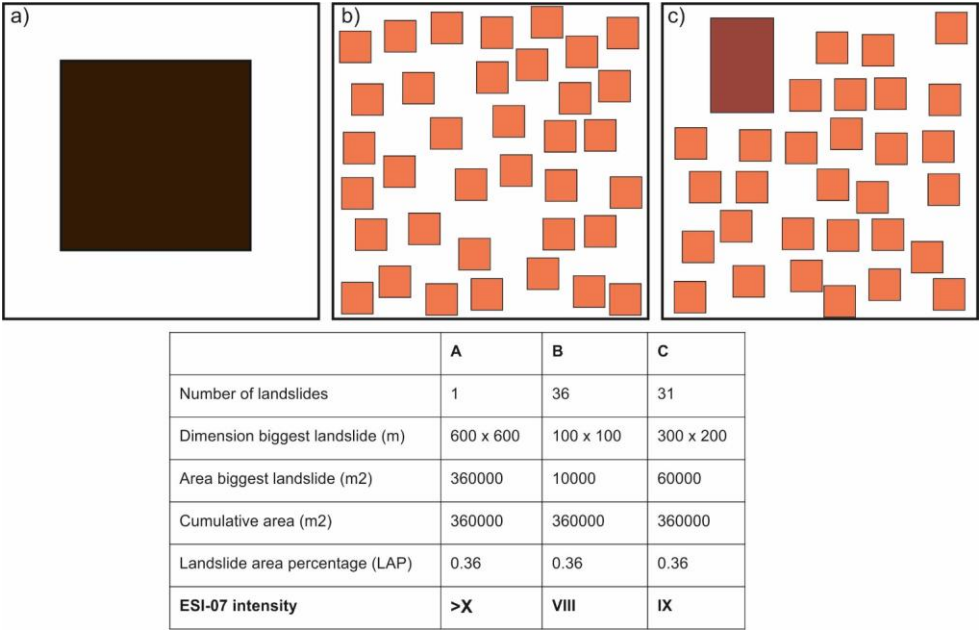|	A	B	C
Number of landslides	1	36	31
Dimension biggest landslide (m)	600 x 600	100 x 100	300 x 200
Area biggest landslide (m2)	360000	10000	60000
Cumulative area (m2)	360000	360000	360000
Landslide area percentage (LAP)	0.36	0.36	0.36
ESI-07 intensity	**>X**	**VIII**	**IX**

165   **Figure 3: Sketch illustrating the role of number and dimension of landslides (coloured squares) on the computation of LND, LAP and ESI-07. The upper panels represent simplified scenarios: a) one wide landslide; b) many landslides, all of small dimension; c) many landslides with variable dimension.**

Finally, the Sabah case study is compared to other landslide inventories on a global scale; in particular, I used the scaling

170   relations of Malamud et al. (2004a, b), which relate the number of triggered landslides, earthquake magnitude and total landslide area:

$$logN = 1.27 \times M - 5.45 \ (\pm 0.46) \quad (2)$$

$$logA_{LT} = 1.27 \times M - 7.96 \ (\pm 0.46) \quad (3)$$

$$A_{LT} = 3.07 \times 10^{-3} \times N \quad (4)$$

175

Where N is the number of landslides, M is <u>moment</u> magnitude and A_{LT} is the total landslide area in km^2. Equations (2) and (3) are from Malamud et al. (2004b), while Equation (4) is from Malamud et al. (2004a).

Table 2: Landslide volumes used in this study to assign ESI-07 local intensities.

ESI-07 degree	VI	VII	VIII	IX	X - XII
Landslide volume (m³)	<10³	10³ – 10⁴	10⁴ – 10⁵	10⁵ – 10⁶	>10⁶

180

4 Results ~~and discussion~~

4.1 Spatial distribution of landslides

The inventory for the 2015 Sabah earthquake comprises 5198 landslides mapped in an 810-km^2 wide area, thus resulting in an average of 6.4 landslides/km^2. Landslides have an average area of 3625 m^2. The slope movements are not equally
185 distributed in space, but instead concentrates in a <u>steep</u> zone ~~of high steepness~~ along the slopes of Mt. Kinabalu (Fig. 2a). Outside the Mt. Kinabalu pluton, landslides clusters in small patches, while the surrounding territory is unaffected. Summing the area of single landslides, a total of 18.84 km^2 is obtained, which represents the 2.33% of the investigated area. Landslides are located north of the epicenter (Fig. 2a), possibly reflecting the rupture directivity which enhanced ground shaking in this direction (Wang et al., 2017).
190 Fig. 3 presents the grid maps of landslide density number (LND) and of landslide area percentage (LAP). Maximum values reach LND = 99 landslides/km^2 and LAP = 68%; the mapped area includes 895 cells, but landslides were mapped only in about 67% of the cells (see the distribution of landslides in Fig. 2a). Overall, there is a good agreement between LND and LAP and the spatial distribution of the two descriptors is fairy similar (Fig. 3). The ~~actual~~ distribution of coseismic landslides can be compared to expected ground failures: the USGS routinely provides such information in the aftermath of
195 strong events, using models based on seismological, topographic and geological variables (Nowicki Jessee et al., 2018). For the Sabah earthquake the model correctly recognizes the slopes of Mt. Kinabalu as the focus of the highest damage and matches fairly well with actual slope movements.
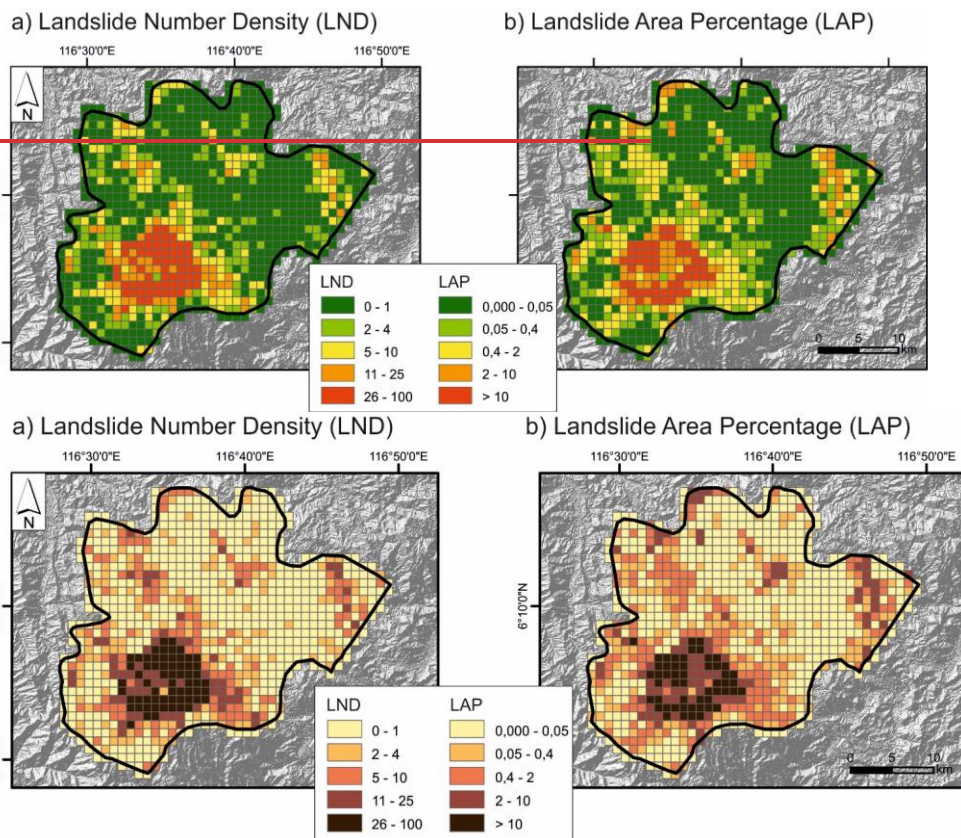
11

Figure 43: Grid maps of Landslide Number Density (LND, a) and Landslide Area Percentage (LAP, b). Colormap follows Crameri et al. (2020).

4.2 Scaling relations among LND, LAP and ESI-07 intensityESI-07 macroseismic field

I compute the landslide volume using Equation (1); in order to test assess the influence of a given scaling relation, I test six seven different models (see Table 1). They encompass different climatic and regional settings and have been derived either from global (Guzzetti et al., 2009; Larsen et al., 2010) or regional (Xu et al., 2016; Massey et al., 2020) datasets. OneTwo of the equations (Xu et al., 2016; Massey et al., 2020) derives from earthquake-induced landslides, while the others refer to

12

landslides triggered by multiple processes (i.e., earthquakes, rainfall, snowmelt). Two of the equations (Benjamin et al., 2018; Caputo et al., 2018) specifically deal with rockfalls.

Fig. 4̶5 presents the grid maps for the s̶i̶x̶ seven scaling relations: when multiple landslides lie in a single cell (i.e., LND > 1), I retain the highest ESI-07 value. Notwithstanding the selected scaling relation, the spatial distribution of ESI-07 values shows a common pattern; this is further summarized in Fig. 4̶g̶5h, where the number of cells belonging to each ESI-07 intensity class is shown for the s̶i̶x̶ seven relations. The Larsen et al. (2010) "soil" regression results in lower intensities than the other equations, while the Xu et al. (2016) regression provides the highest number of cells with intensity ≥ VIII. The number of cells having an ESI-07 intensity ≥ X ranges from 2 (Larsen et al., 2010 "soil") to 28 (G̶u̶z̶z̶e̶t̶t̶i̶ ̶e̶t̶ ̶a̶l̶.̶,̶ ̶2̶0̶0̶9̶;̶ Xu et al., 2016), which represent the 0.2 – 3.1% of the total cells.

One limitation of the equations specific for rockfalls (Benjamin et al., 2018 and Caputo et al., 2018) is the dimension of the individual rockfalls, which in both cases do not exceed 30 m^2. The extrapolation of the A-V relations to much bigger landslides should be carefully considered; nevertheless, the 7 relations considered in this study clearly show a similar picture in terms of ESI-07 distribution, testifying T̶h̶e̶ ̶c̶o̶m̶p̶a̶r̶a̶b̶l̶e̶ ̶d̶i̶s̶t̶r̶i̶b̶u̶t̶i̶o̶n̶ ̶o̶f̶ ̶E̶S̶I̶-̶0̶7̶ ̶v̶a̶l̶u̶e̶s̶ ̶d̶e̶m̶o̶n̶s̶t̶r̶a̶t̶e̶s̶ that input data (i.e., landslide inventory) are far more important tha̶n̶t the choice of the area-volume relation.
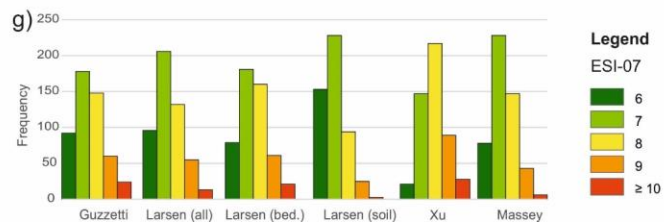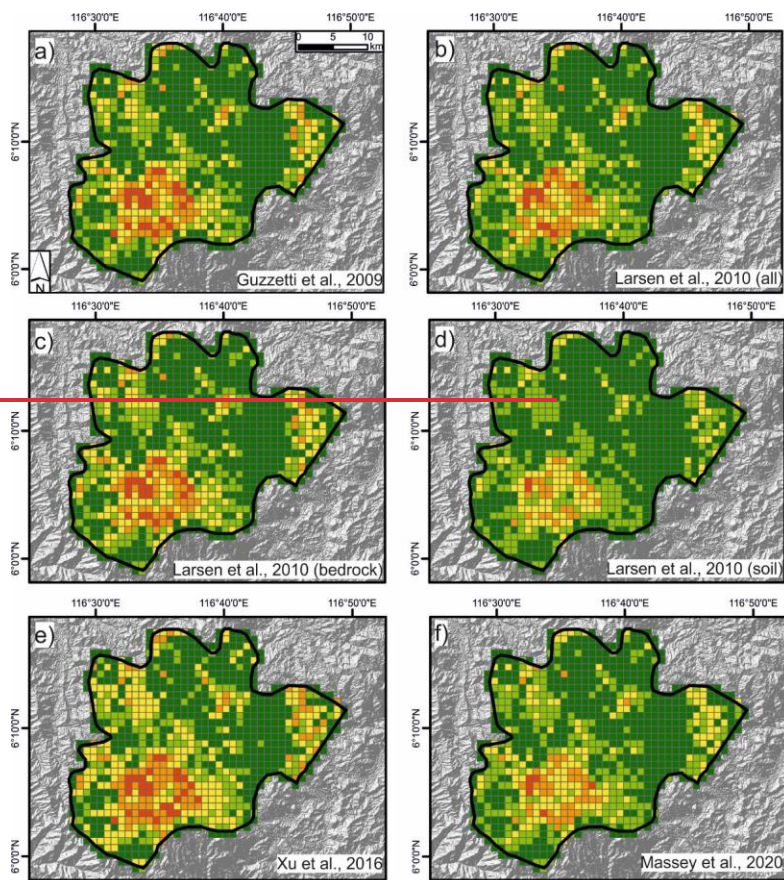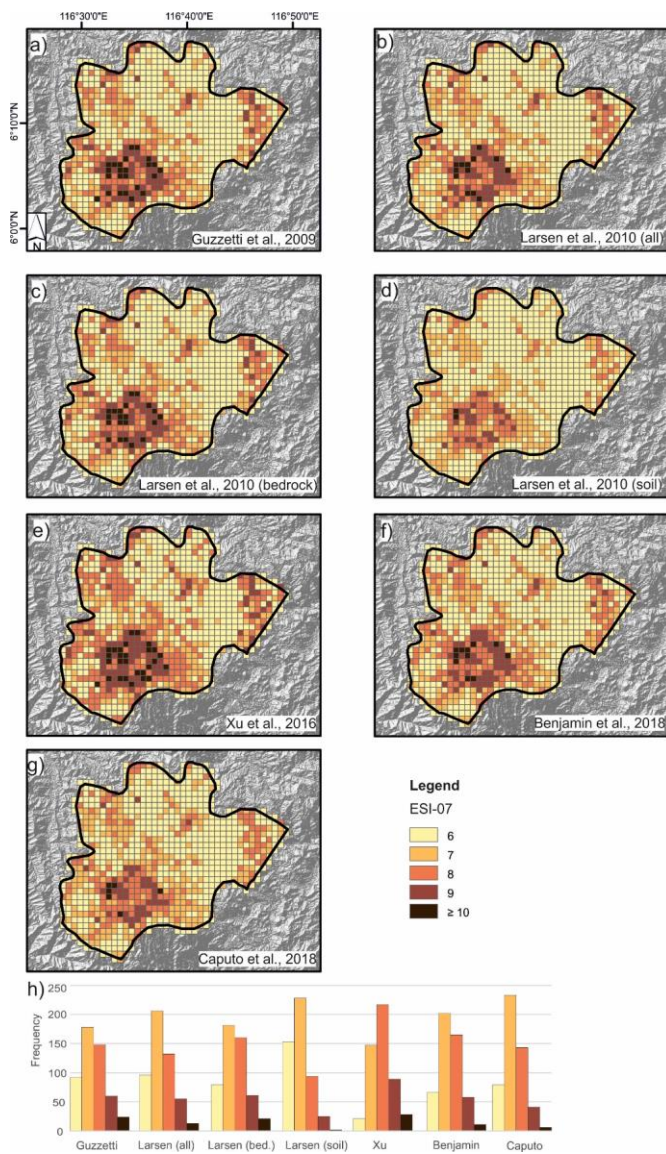
Figure 4: **Grid maps of ESI-07 local intensity obtained by adopting different area-volume scaling relations.**

LND and LAP have been frequently explored in the realm of earthquake-triggered landslide inventories (e.g., Fan et al., 2018; Ferrario, 2019; Ghaedi Vanani et al., 2021; Xu et al., 2014), while a grid approach has been seldom applied in the assessment of ESI-07 intensity, with the exceptions of Ota et al. (2009) and Silva et al. (2013). The current work is the first attempt toward a quantitative relation among LND/LAP and ESI-07. In Fig. 5 I show the distribution of ESI-07 intensity with respect to LND and LAP values of each grid cell. The graphs refer to the results obtained with the Guzzetti et al. (2009) equation, but a similar picture is obtained when applying the other equations of Table 1.

The median LND and LAP values for each ESI-07 intensity class are presented in Table 3: it can be noticed that in some instances (Larsen et al., 2010 "bedrock" and "soil"; Massey et al., 2020) LND values for the ESI-07 class IX are higher than X, but this inversion is possibly driven by the limited number of cells in the ESI-07 X class. Median LAP values instead do not show such inversions, eventually suggesting that LAP is a better descriptor than LND for assessing the damage. This fact is not surprising, since LND has a "point" validity, while LAP is by definition intimately related to an area assessment. Additionally, LAP may be more stable than LND with respect to epistemic uncertainty, because the number of mapped landslides (and thus LND) is strongly dependent from the resolution of images used for building the inventory.

a) LND vs ESI-07
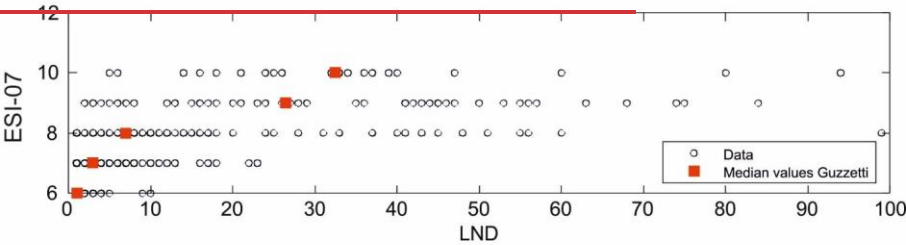
b) LAP vs ESI-07
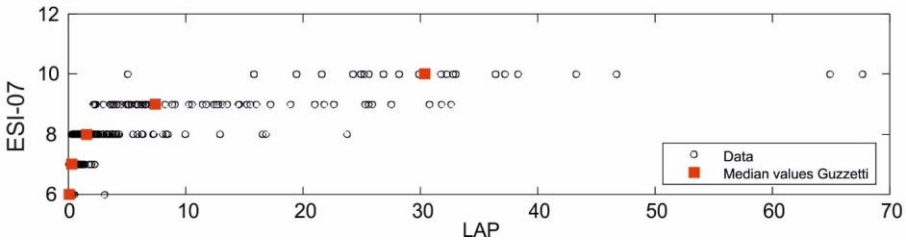
16

Figure 5: Plots of LND (a) and LAP (b) vs local ESI-07; intensity computed using the Guzzetti et al. (2009) scaling relation is shown as an example.

Table 3: Median values of LND and LAP for each ESI-07 intensity degree, obtained using the area-volume scaling relations of Table 1.

	Landslide Number Density						Landslide Area Percentage					
ESI-07	Guzzetti	Larsen (all)	Larsen (bedrock)	Larsen (soil)	Xu	Massey	Guzzetti	Larsen (all)	Larsen (bedrock)	Larsen (soil)	Xu	Massey
VI	1	1	1	2	1	1	0.049	0.050	0.041	0.088	0.022	0.041
VII	3	3	3	5	2	3	0.279	0.337	0.241	0.697	0.105	0.317
VIII	7	8	7	17	5	9	1.552	1.911	1.529	5.761	0.742	2.279
IX	27	29	27	33	17	35	7.391	13.548	8.229	29.852	5.867	21.600
≥X	33	26	32	23	33	23	30.354	33.020	30.355	55.477	30.103	44.992

5 Discussion

5.1 Challenges and data limitations

The Sabah earthquake and the methodological approach presented in this study highlight some of the challenges commonly encountered when analyzing earthquake-induced landslide inventories. Indeed, the realization of a reliable landslide inventory requires the fulfilment of several criteria, either in terms of available images or mapping methodology (Harp et al., 2011). In this section, I discuss the role of pre-existing landslides, i.e., slope movements already present before the Sabah earthquake (Section 5.1.1) and other sources of epistemic uncertainty (Section 5.1.2).

5.1.1 The role of pre-existing landslides

A co-seismic landslide inventory should include only those slope movements triggered, or reactivated, by the seismic shaking. The inventory presented in this paper is realized on a homogeneous dataset of satellite images provided by PlanetScope; similar images are not available for the timeframe antecedent the earthquake, introducing a difficulty in the evaluation of whether a landslide was already present before the earthquake. Thus, I realized a dataset of pre-existing landslides by inspecting Google Earth historical images, ranging from 19 May 2008 to 2 June 2015. Cloud-free images are not available for a 186 km^2 wide region, corresponding to 23% of the total area (blue region in Fig. 6). I mapped a total of 225 pre-existing landslides and compute LND and LAP with the same procedure adopted for the co-seismic inventory. It is evident that pre-existing landslides exert a very limited role, either in terms of total number (225 pre-existing vs 5198 co-seismic) and area (0.55 vs 18.84 km^2). In Fig. 6, I adopted the same color scheme as for the co-seismic inventory (Fig. 4), to

highlight that more than 95% of the grid cells belong to the lowest LND class (less than 2 landslides per cell), while more than 99% of the cells belong to the lowest LAP class (max LAP value is 0.09%).
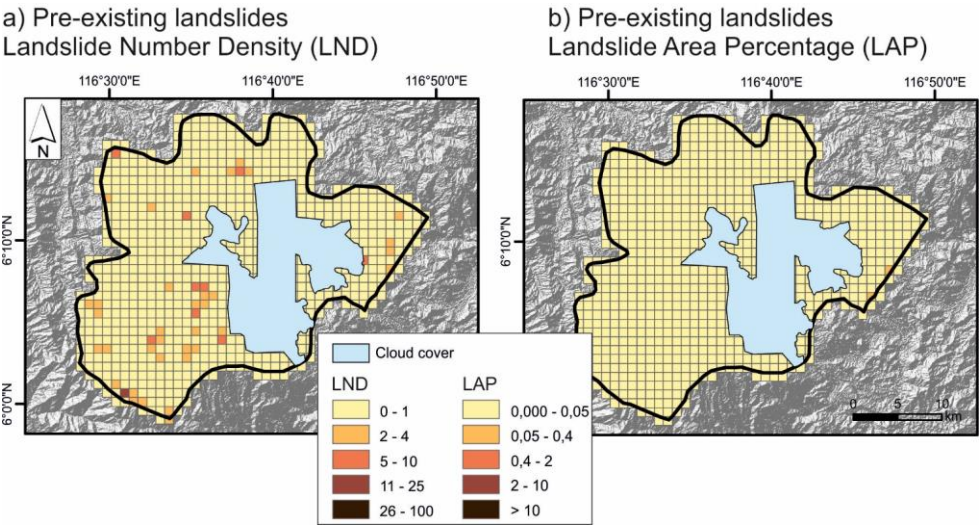

Figure 6: Grid maps of Landslide Number Density (LND, a) and Landslide Area Percentage (LAP, b) for pre-existing landslides; the blue area represents a region where cloud-free pre-earthquake imagery is lacking. Colormap follows Crameri et al. (2020).

5.1.2 Chain of hazards and other sources of epistemic uncertainty

Several processes can trigger landslides, such as seismic shaking, heavy rainfall, anthropic disturbances. These processes may act concurrently or have complex interdependencies among each other, resulting in a so-called chain of hazards (e.g., Fan et al., 2019). The identification of the precise event that triggered the landslides can be challenging, and subsequent remobilizations may occur as well. In the Sabah case, slope movements were firstly triggered by the seismic shaking; later on, prolonged rainfall reactivated the landslide deposits as debris flows (Rosli et al., 2021a). In this work, landslides were mapped on optical satellite images, whose availability depends on satellite revisit time and local weather conditions. The co-seismic landslide inventory is realized on images acquired about 8 months after the Sabah earthquake, since persistent cloud cover hampered the analysis of a shorter time interval. This point is a significant source of epistemic uncertainty, which is difficult to reduce, unless other data sources are present (e.g., field surveys, helicopter/drone flights).

Chain of hazards affect the territory for prolonged times: tThe remobilization of deposits results in enhanced rates of slope movements; these processes may take 5-10 years (Avsar et al., 2016) and generate bank erosion or floodplain accretion downstream, thus affecting flood frequency (Fan et al., 2019). Stochastic natural processes (e.g., earthquakes) and seasonal hazards (e.g., rainfall, flood) imply different modeling tools and calls for complex risk reduction strategies (Quigley et al., 2020); understanding cause-effect relationships and latent vulnerabilities helps in informing such efforts (Pescaroli & Alexander, 2016). Additionally, landslide phenomena triggered by human activities are increasing and have an influence comparable, if not higher, than natural processes such as rainfall or earthquakes (Froude & Petley, 2018; Tanyas et al., 2022). The identification of critical nodes and interdependencies among cascading hazards can be beneficial for the development of targeted mitigation strategies.

Another source of epistemic uncertainty is related to the area-volume scaling relations adopted to compute ESI-07 values. Many equations have been proposed in the literature, referring to different triggering processes (e.g., seismic shaking vs rainfall), climate conditions (specific regions vs global validity), landslide type (slides vs rockfall), mapping procedures (e.g., landslides delineated as single polygons vs separation of source and deposit area) and methods for data acquisition (e.g., manual vs automatic mapping; satellite vs drone images vs laser scanner techniques). Thus, the selection of the most suitable equation may not be straightforward. In Section 4.2 I used seven different equations to derive the ESI-07 macroseismic field; results demonstrate that the epistemic uncertainty related to the choice of the area-volume relation is much lower than other sources of uncertainty.

The derivation of reliable scaling relations among ESI-07 intensity and LND/LAP cannot be based on the single case study of the Sabah earthquake. Scaling relations are expected to have a regional validity and thus it is necessary to investigate the inter-event variability (i.e., comparison among different earthquakes), by considering earthquakes occurred in different seismotectonic and climatic settings.

The categorization of LND and LAP values may be useful to investigate the variable degree of damage on the territory. Xu et al. (2013) propose numerical thresholds to correlate LND and LAP with macroseismic intensity (Chinese scale) following the 2008 Wenchuan earthquake. Hancox et al. (2002) included information on landslides triggered by historical earthquakes in New Zealand for assigning intensities on the Modified Mercalli (MM) scale. Beyond earthquake-induced landslides, Bessette-Kirton et al. (2019) analyzed failures triggered in Puerto Rico (US) by Hurricane Maria using a 2 km x 2 km grid; they classified the territory as either having no landslides, low density (1-25 landslides/km^2) and high density (> 25 landslides/km^2).

In Fig. 6, the median LND and LAP values (see Table 3) derived for the Sabah earthquake are compared to the thresholds proposed by Xu et al. (2013). A striking inter-event variability can be noticed: the difference between Wenchuan and Sabah earthquakes is much higher than the influence of the area-volume relation used to assess ESI-07 intensities. One limitation of the data in Fig. 6 is that ESI-07 and Chinese intensity scales are not fully comparable. Inter-event variability is not surprising, and a more comprehensive assessment may be the focus of future efforts: as a research hypothesis, I propose to apply the workflow presented here for the Sabah case to several inventories of earthquake-triggered landslides (Schmitt et

19

al., 2017; Tanyas et al., 2017). The ESI-07 scale seems the most appropriate classification, since it is based only on EEEs and it has a global validity. A statistical approach can then be pursued, investigating either the intra-event (e.g., dispersion of LND and LAP values for each intensity class) and inter-event (comparison among different earthquakes) variability. Geostatistical models (e.g., Lombardo et al., 2021) could be applied as well.
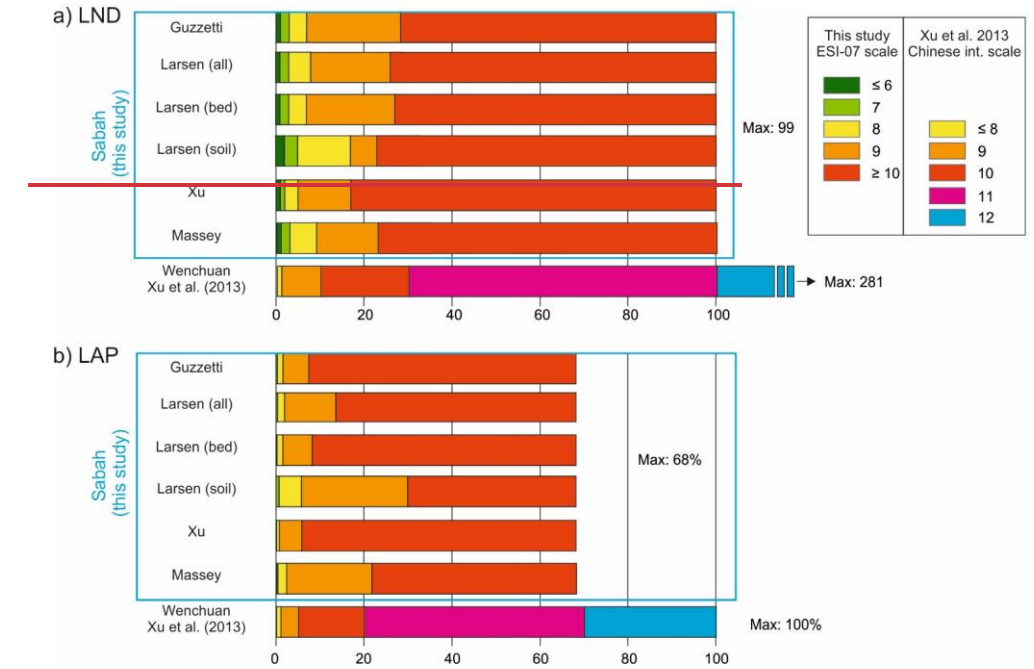

Figure 6: Comparison among LAP and LND classes proposed for the Sabah and Wenchuan earthquakes (this study and Xu et al., 2013, respectively). This study adopts the ESI-07 scale, while the classes by Xu et al. (2013) refer to the Chinese intensity scale.

LND and LAP have been frequently explored in the realm of earthquake-triggered landslide inventories (e.g., Fan et al., 2018; Ferrario, 2019; Ghaedi Vanani et al., 2021; Xu et al., 2014), while a grid approach has been seldom applied in the assessment of ESI-07 intensity, with the exceptions of Ota et al. (2009) and Silva et al. (2013). The current work is the first attempt toward a quantitative relation among LND/LAP and ESI-07.

20

4.35.2 Comparing the 2015 Sabah case study with worldwide data

Here I compare the Sabah case study to other landslide inventories on a global scale, to evaluate its characteristics in a broader context; eventual peculiar characteristics are then discussed. Fig. 7 summarizes the characteristics of a number of earthquake-triggered landslide inventories, represented as a function of earthquake moment magnitude. Open symbols represent data collected from published literature; the dataset is available on the Zenodo repository (see Data availability section). Fig. 7a shows the number of triggered landslides with respect to Mw; Equation (2) and its confidence bounds are shown as well. The Sabah case history lies well above the expected value, probably because it includes both strictly earthquake-triggered landslides and material remobilized by subsequent debris flows (Rosli et al., 2021a, b). Fig. 7b shows the dimension of the area affected by landslides; in this case, the Sabah inventory is in good agreement with global studies and lies just below the upper bound proposed by Keefer (1984; solid line). Fig. 7c presents the total landslide area (sum of areas of individual landslides), together with Equation (3) and relative confidence bounds; the Sabah earthquake seems an outlier in the data population, although the debris flow remobilization may make the landslide area estimate not fully reliable for the Sabah earthquake. On the contrary, by adopting the relation based on number of landslides (i.e., Equation 4), the expected landslide area of 15.96 km^2 is in fair agreement with the observed value of 18.84 km^2. It must be noted that the works by Keefer (1984) and Malamud et al. (2004b) were based on a subset of the datapoints in Fig. 7; many inventories were realized in the last few years, possibly arguing for the need of updating the scaling relations. Nevertheless, for a given Mw the plots show a high variability, spanning about 3 orders of magnitude in terms of number of landslides, affected area and landslide area. Such behavior is related to inherent variability in landslide occurrence across varying geological settings: the local conditions play a prominent role in driving secondary earthquake environmental effects (Keefer, 2002; Michetti et al., 2007; Fan et al., 2019). Finally, Fig. 7d shows the distribution of ESI-07 epicentral intensity as a function of Mw (Ferrario et al., 2022). The ESI-07 epicentral intensity is assigned based either on the dimension of the affected area, or on the dimension of the biggest effects. I assign an ESI-07 epicentral intensity of IX to the Sabah case history: the area encompassing all the mapped landslides is 810-km^2 wide, which fits the description in the ESI-07 guidelines (*"the affected area is usually less than 1000 km^2"*; Michetti et al., 2004). The Sabah case study is widely in agreement with the dataset.
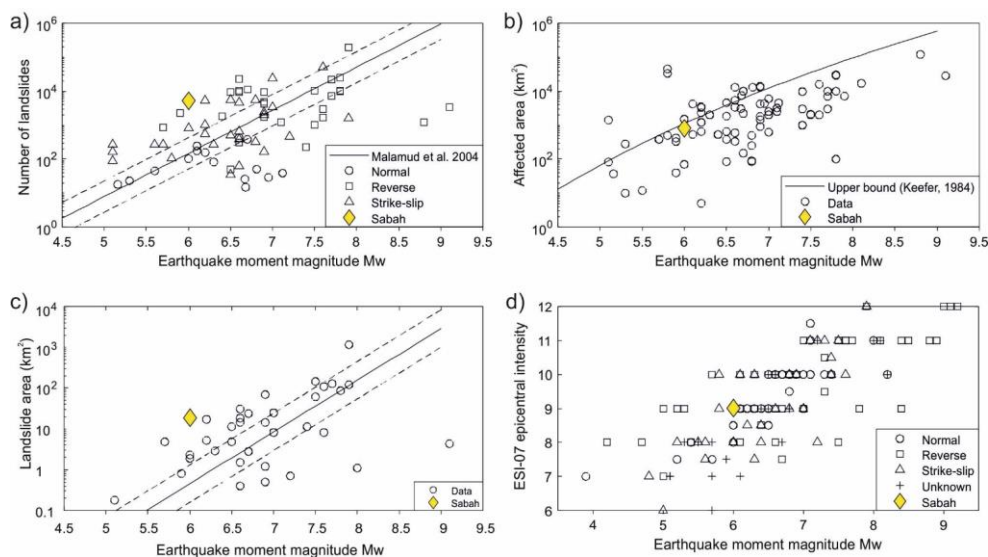
Figure 7: Comparison of the Sabah earthquake with global studies: a) number of landslides vs Mw, regression is Equation (2); b) affected area vs Mw, upper bound after Keefer, 1984; c) landslide area vs Mw, regression is Equation (3); d) ESI-07 epicentral intensity.

360 The Sabah earthquake produced a higher number of slope movements and a higher landslide area (sum of areas of individual landslides) than events of similar magnitude. This fact can be related to two alternative explanations:

- The 2015 earthquake is the strongest event in Sabah in the instrumental era: infrequent strong events may be highly efficient in triggering a large number of landslides.

365 - I realized the inventory on satellite images acquired 8 months after the earthquake, thus slope movements triggered by processes other than the mainshock may be included, such as debris flow remobilization.

- The latter point highlights the challenge of documenting chains of hazards: indeed, prolonged rainfall reactivated the landslide deposits as debris flows (Rosli et al., 2021); if the chain of hazards occurs in a short time interval (e.g., few days), only the cumulative damage can be assessed. The remobilization of deposits results in enhanced rates of slope movements; these processes may take 5-10 years (Avsar et al., 2016) and generate bank erosion or floodplain

370 accretion downstream, thus affecting flood frequency (Fan et al., 2019). Stochastic natural processes (e.g., earthquakes) and seasonal hazards (e.g., rainfall, flood) imply different modeling tools and calls for complex risk reduction strategies (Quigley et al., 2020); understanding cause-effect relationships and latent vulnerabilities helps in informing such efforts (Pescaroli & Alexander, 2016). Additionally, landslide phenomena triggered by human

~~activities are increasing and have an influence comparable, if not higher, than natural processes such as rainfall or earthquakes (Froude & Petley, 2018; Tanyas et al., 2022).~~

5.3 Scaling relations among LND, LAP and ESI-07

In Fig. 8 I show the distribution of ESI-07 intensity with respect to LND and LAP values of each grid cell. The graphs refer to the results obtained with the Guzzetti et al. (2009) equation, but a similar picture is obtained when applying the other equations of Table 1. The median LND and LAP values for each ESI-07 intensity class are presented in Table 3 and Table 4: it can be noticed that in some instances (Larsen et al., 2010 "bedrock" and "soil"; Caputo et al., 2018) LND values for the ESI-07 class IX are higher than X, but this inversion is possibly driven by the limited number of cells in the ESI-07 X class. Median LAP values instead do not show such inversions, eventually suggesting that LAP is a better descriptor than LND for assessing the damage. This fact is not surprising, since LND has a "point" validity, while LAP is by definition intimately related to an area assessment. Additionally, LAP may be more stable than LND with respect to epistemic uncertainty, because the number of mapped landslides (and thus LND) is strongly dependent on the resolution of images used for building the inventory and may be affected by amalgamation issues (Marc & Hovius, 2015).
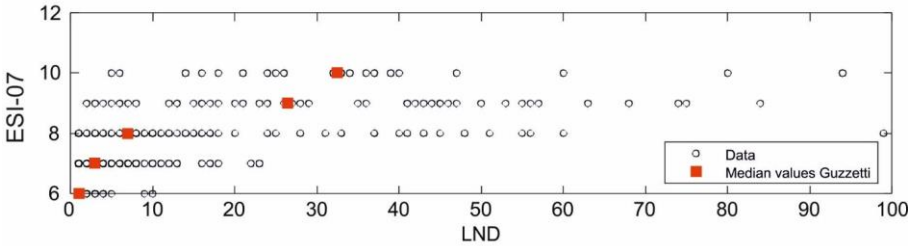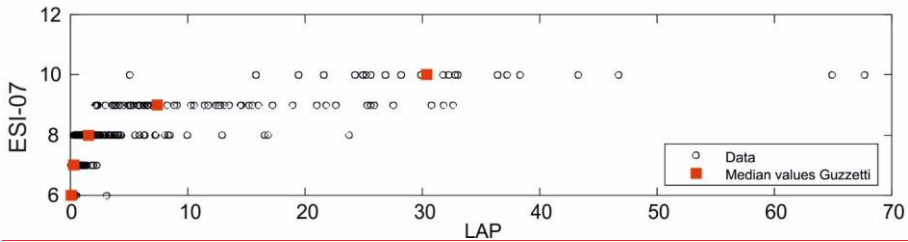
Figure 8: Plots of LND (a) and LAP (b) vs local ESI-07; intensity computed using the Guzzetti et al. (2009) scaling relation is shown as an example.

Table 3: Median values of LND for each ESI-07 intensity degree, obtained using the area-volume scaling relations of Table 1.

ESI-07	Guzzetti	Larsen (all)	Larsen (bedrock)	Larsen (soil)	Xu	Benjamin	Caputo
VI	1	1	1	2	1	1	1
VII	3	3	3	5	2	2	3
VIII	7	8	7	17	5	8	9
IX	27	29	27	33	17	29	35
≥ X	33	26	32	23	33	32	22

Table 4: Median values of LAP for each ESI-07 intensity degree, obtained using the area-volume scaling relations of Table 1.

ESI-07	Guzzetti	Larsen (all)	Larsen (bedrock)	Larsen (soil)	Xu	Benjamin	Caputo
VI	0.049	0.050	0.041	0.088	0.022	0.038	0.041
VII	0.279	0.337	0.241	0.697	0.105	0.238	0.331

24

VIII	1.552	1.911	1.529	5.761	0.742	1.696	2.346
IX	7.391	13.548	8.229	29.852	5.867	14.023	22.616
≥ X	30.354	33.020	30.355	55.477	30.103	33.02	44.992

5.4 Prospect for future work

LND and LAP have been frequently explored in the realm of earthquake-triggered landslide inventories (e.g., Fan et al., 2018; Ferrario, 2019; Ghaedi Vanani et al., 2021; Xu et al., 2014), while a grid approach has been seldom applied in the assessment of ESI-07 intensity, with the exceptions of Ota et al. (2009) and Silva et al. (2013). The current work is the first attempt toward a quantitative relation among LND/LAP and ESI-07. In Section 5.3, I describe the relations obtained for the Sabah earthquake; nevertheless, reliable empirical relations should be based on a wider dataset and not on a single case history. Scaling relations are indeed expected to have a regional validity and thus it is necessary to investigate the inter-event variability (i.e., comparison among different earthquakes), by considering earthquakes occurred in different seismotectonic and climatic settings.

The categorization of LND and LAP values may be useful to investigate the variable degree of damage on the territory. Xu et al. (2013) propose numerical thresholds to correlate LND and LAP with macroseismic intensity (Chinese scale) following the 2008 Wenchuan earthquake. Hancox et al. (2002) included information on landslides triggered by historical earthquakes in New Zealand for assigning intensities on the Modified Mercalli (MM) scale. Beyond earthquake-induced landslides, Bessette-Kirton et al. (2019) analyzed failures triggered in Puerto Rico (US) by Hurricane Maria using a 2 km x 2 km grid; they classified the territory as either having no landslides, low density (1-25 landslides/km^2) and high density (> 25 landslides/km^2).

In Fig. 9, the median LND and LAP values derived for the Sabah earthquake are compared to the thresholds proposed by Xu et al. (2013). A striking inter-event variability can be noticed: the difference between Wenchuan and Sabah earthquakes is much higher than the influence of the area-volume relation used to assess ESI-07 intensities. One limitation of the data in Fig. 9 is that ESI-07 and Chinese intensity scales are not fully comparable. Inter-event variability is not surprising, and a more comprehensive assessment may be the focus of future efforts: as a research hypothesis, I propose to apply the workflow presented here for the Sabah case to several inventories of earthquake-triggered landslides (Schmitt et al., 2017; Tanyas et al., 2017). The ESI-07 scale seems the most appropriate classification, since it is based only on earthquake environmental effects, and it has a global validity. A statistical approach can then be pursued, investigating either the intra-event (e.g., dispersion of LND and LAP values for each intensity class) and inter-event (comparison among different earthquakes) variability. Geostatistical models (e.g., Lombardo et al., 2021) could be applied as well.

The methodological workflow presented here can be applied to other case histories, to obtain more reliable scaling relations among LND/LAP and ESI-07, eventually tuned according to climatic or seismological parameters, or to the type of slope movement or hillslope material. One way to measure the impact of the methodological workflow presented in this research is

25

its eventual implementation into near real-time products. Currently, Shakemaps and ground failure models are routinely produced following strong earthquakes; these maps provide information on the expected ground motion (expressed in terms of Modified Mercalli intensity, PGA or PGV) and environmental effects (landslides and liquefaction). A similar map expressed in terms of ESI-07 intensity could be an added value with respect to the extant practice.
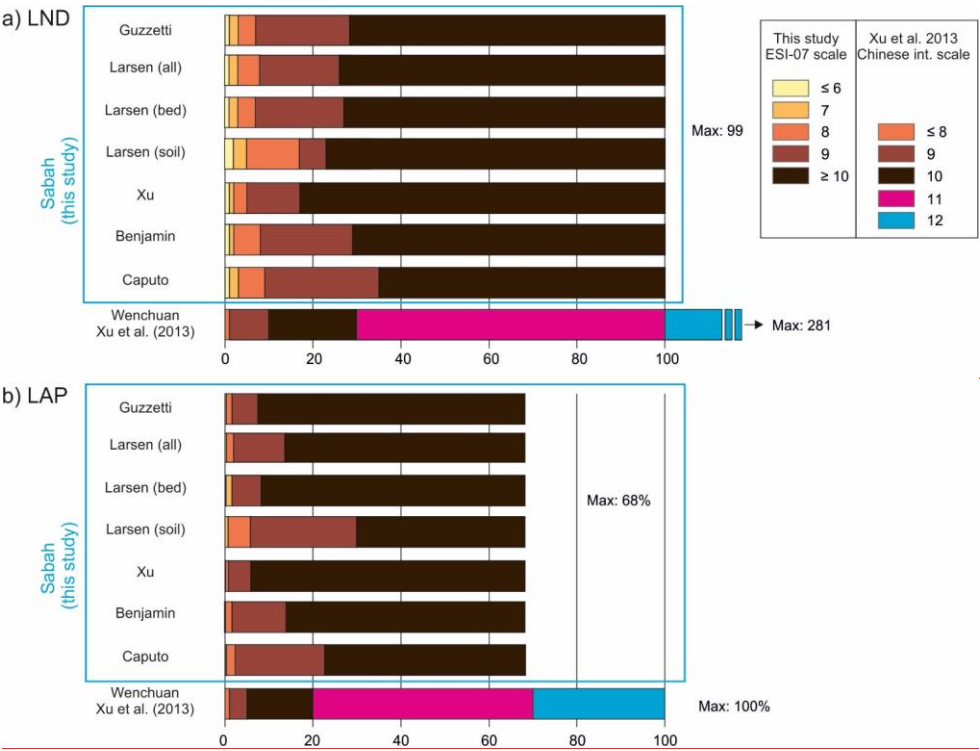
430

Figure 9: Comparison among LAP and LND classes proposed for the Sabah and Wenchuan earthquakes (this study and Xu et al., 2013, respectively). This study adopts the ESI-07 scale, while the classes by Xu et al. (2013) refer to the Chinese intensity scale.

435

5 6 Conclusions

In this paper, I present an inventory of 5198 landslides triggered by the Mw 6.0 Sabah earthquake, occurred on 4 June 2015. I investigate the spatial pattern of landslides by means of the Landslide Number Density (LND) and the Landslide Area Percentage (LAP) on a regular grid of 1-km^2 cells. I estimate the ESI-07 intensity for each cell taking advantage of published area-volume scaling relations and demonstrating that the epistemic uncertainty related to the chosen equation has limited implications on the final output.

I compare the Sabah earthquake with other events on a global scale, finding a good correspondence in terms of total affected area and ESI-07 intensity. I believe that the methodological workflow presented in this paper can be successfully exported in other territorial settings and that joining scientific communities that rarely share their results (e.g., communities responsible for the realization of inventories and for ESI-07 scale assessment) is beneficial for a more comprehensive understanding of the overall earthquake damage.

Declaration of competing interests: The authors declare that they have no conflict of interest.

References

Avşar, U., Jónsson, S., Avşar, Ö., and Schmidt, S.: Earthquake-induced soft-sediment deformations and seismically amplified erosion rates recorded in varved sediments of Köyceğiz Lake (SW Turkey): Earthquake Records in Lacustrine Varves, J. Geophys. Res. Solid Earth, 121, 4767–4779, https://doi.org/10.1002/2016JB012820, 2016.

Benjamin, J., Rosser, N. J., and Brain, M. J.: Rockfall detection and volumetric characterisation using LiDAR. In *Landslides and Engineered Slopes. Experience, Theory and Practice* (pp. 389-395). CRC Press, 2018.

470 Bessette-Kirton, E. K., Cerovski-Darriau, C., Schulz, W. H., Coe, J. A., Kean, J. W., Godt, J. W., Thomas, M. A. and Hughes, K. S.: Landslides triggered by Hurricane Maria: Assessment of an extreme event in Puerto Rico, GSAT, 29, 4–10, https://doi.org/10.1130/GSATG383A.1, 2019.

Budimir, M. E. A., Atkinson, P. M., and Lewis, H. G.: Earthquake-and-landslide events are associated with more fatalities than earthquakes alone, Nat Hazards, 72, 895–914, https://doi.org/10.1007/s11069-014-1044-4, 2014.

475 Burrows, K., Walters, R. J., Milledge, D., and Densmore, A. L.: A systematic exploration of satellite radar coherence methods for rapid landslide detection, Nat. Hazards Earth Syst. Sci., 20, 3197–3214, https://doi.org/10.5194/nhess-20-3197-2020, 2020.

Caputo, T., Marino, E., Matano, F., Somma, R., Troise, C., and De Natale, G.: Terrestrial Laser Scanning (TLS) data for the analysis of coastal tuff cliff retreat: application to Coroglio cliff, Naples, Italy. Annals of Geophysics, 61(1), 2018.

480 Cecić, I. and Musson, R.: Macroseismic surveys in theory and practice. Nat. Haz., 31(1), 39-61, 2004.

Chang, M., Zhou, Y., Zhou, C., and Hales, T. C.: Coseismic landslides induced by the 2018 Mw 6.6 Iburi, Japan, Earthquake: spatial distribution, key factors weight, and susceptibility regionalization, Landslides, 18, 755–772, https://doi.org/10.1007/s10346-020-01522-3, 2021.

Crameri, F., Shephard, G. E., and Heron, P. J.: The misuse of colour in science communication. Nature communications, 11(1), 1-10, https://doi.org/10.1038/s41467-020-19160-7, 2020.

485 Cottam, M., Hall, R., Sperber, C., and Armstrong, R.: Pulsed emplacement of the Mount Kinabalu granite, northern Borneo, Journal of the Geological Society, 167, 49–60, https://doi.org/10.1144/0016-76492009-028, 2010.

Fan, X., Scaringi, G., Xu, Q., Zhan, W., Dai, L., Li, Y., Pei, X., Yang, Q., and Huang, R.: Coseismic landslides triggered by the 8th August 2017 Ms 7.0 Jiuzhaigou earthquake (Sichuan, China): factors controlling their spatial distribution and 490 implications for the seismogenic blind fault identification, Landslides, 15, 967–983, https://doi.org/10.1007/s10346-018-0960-x, 2018.

Fan, X., Scaringi, G., Korup, O., West, A. J., Westen, C. J., Tanyas, H., Hovius, N., Hales, T. C., Jibson, R. W., Allstadt, K. E., Zhang, L., Evans, S. G., Xu, C., Li, G., Pei, X., Xu, Q., and Huang, R.: Earthquake-Induced Chains of Geologic Hazards: Patterns, Mechanisms, and Impacts, Rev. Geophys., 57, 421–503, https://doi.org/10.1029/2018RG000626, 2019.

495 Ferrario, M. F.: Landslides triggered by multiple earthquakes: insights from the 2018 Lombok (Indonesia) events, Nat Hazards, 98, 575–592, https://doi.org/10.1007/s11069-019-03718-w, 2019.

Ferrario, M. F., Livio, F., and Michetti, A. M.: Fifteen years of Environmental Seismic Intensity (ESI-07) scale: Dataset compilation and insights from empirical regressions. Quaternary International, 2022.

Froude, M. J. and Petley, D. N.: Global fatal landslide occurrence from 2004 to 2016, Nat. Hazards Earth Syst. Sci., 18, 500 2161–2181, https://doi.org/10.5194/nhess-18-2161-2018, 2018.

Ghaedi Vanani, A. A., Shoaei, G., and Zare, M.: Statistical analyses of landslide size and spatial distribution triggered by 1990 Rudbar-Manjil (Mw 7.3) earthquake, northern Iran: revised inventory, and controlling factors, Bull Eng Geol Environ, 80, 3381–3403, https://doi.org/10.1007/s10064-021-02106-8, 2021.

Guzzetti, F., Ardizzone, F., Cardinali, M., Rossi, M., and Valigi, D.: Landslide volumes and landslide mobilization rates in Umbria, central Italy, Earth and Planetary Science Letters, 279, 222–229, https://doi.org/10.1016/j.epsl.2009.01.005, 2009.

Hall, R.: Contraction and extension in northern Borneo driven by subduction rollback, Journal of Asian Earth Sciences, 76, 399–411, https://doi.org/10.1016/j.jseaes.2013.04.010, 2013.

Hancox, G. T., Perrin, N. D., and Dellow, G. D.: Recent studies of historical earthquake-induced landsliding, ground damage, and MM intensity in New Zealand, BNZSEE, 35, 59–95, https://doi.org/10.5459/bnzsee.35.2.59-95, 2002.

Handwerger, A. L., Jones, S. Y., Huang, M.-H., Amatya, P., Kerner, H. R., and Kirschbaum, D. B.: Rapid landslide identification using synthetic aperture radar amplitude change detection on the Google Earth Engine, Landslides and Debris Flows Hazards, https://doi.org/10.5194/nhess-2020-315, 2020.

Harp, E. L., Keefer, D. K., Sato, H. P., and Yagi, H.: Landslide inventories: The essential part of seismic landslide hazard analyses, Engineering Geology, 122, 9–21, https://doi.org/10.1016/j.enggeo.2010.06.013, 2011.

Harrison, C. G. and Williams, P. R.: A systems approach to natural disaster resilience, Simulation Modelling Practice and Theory, 65, 11–31, https://doi.org/10.1016/j.simpat.2016.02.008, 2016.

Hutchison, C. S., Bergman, S. C., Swauger, D. A., and Graves, J. E.: A Miocene collisional belt in north Borneo: uplift mechanism and isostatic adjustment quantified by thermochronology, Journal of the Geological Society, 157, 783–793, https://doi.org/10.1144/jgs.157.4.783, 2000.

Keefer, D. K.: Landslides caused by earthquakes, GSA Bulletin, GeoScienceWorld, [online] Available from: https://pubs.geoscienceworld.org/gsa/gsabulletin/article-abstract/95/4/406/202914, 1984.

Keefer, D.K.: Investigating landslides caused by earthquakes – a historical review. Surv Geophys 23(6):473–510. https://doi.org/10.1023/A:1021274710840, 2002.

Larsen, I. J., Montgomery, D. R., and Korup, O.: Landslide erosion controlled by hillslope material, Nature Geosci, 3, 247–251, https://doi.org/10.1038/ngeo776, 2010.

Lehan, N. F. A. M., Razak, K. A. and Kamarudin, K. H.: Business continuity and resiliency planning in disaster prone area of Sabah, Malaysia. Disaster Advances, 13(7), 25-32, 2020.

Lombardo, L., Tanyas, H., Huser, R., Guzzetti, F., and Castro-Camilo, D.: Landslide size matters: A new data-driven, spatial prototype, Engineering Geology, 293, 106288, https://doi.org/10.1016/j.enggeo.2021.106288, 2021.

Malamud, B. D., Turcotte, D. L., Guzzetti, F., and Reichenbach, P.: Landslide inventories and their statistical properties, Earth Surf. Process. Landforms, 29, 687–711, https://doi.org/10.1002/esp.1064, 2004a.

Malamud, B. D., Turcotte, D. L., Guzzetti, F., and Reichenbach, P.: Landslides, earthquakes, and erosion, Earth and Planetary Science Letters, 229, 45–59, https://doi.org/10.1016/j.epsl.2004.10.018, 2004b.

Marano, K. D., Wald, D. J., and Allen, T. I.: Global earthquake casualties due to secondary effects: a quantitative analysis

535   for improving rapid loss analyses, Nat Hazards, 52, 319–328, https://doi.org/10.1007/s11069-009-9372-5, 2010.

Marc, O. and Hovius, N.: Amalgamation in landslide maps: effects and automatic detection, Nat. Hazards Earth Syst. Sci., 15, 723–733, https://doi.org/10.5194/nhess-15-723-2015, 2015.

Massey, C. I., Townsend, D., Jones, K., Lukovic, B., Rhoades, D., Morgenstern, R., Rosser, B., Ries, W., Howarth, J., Hamling, I., Petley, D., Clark, M., Wartman, J., Litchfield, N., and Olsen, M.: Volume Characteristics of Landslides

540   Triggered by the M $_W$ 7.8 2016 Kaikōura Earthquake, New Zealand, Derived From Digital Surface Difference Modeling, J. Geophys. Res. Earth Surf., 125, https://doi.org/10.1029/2019JF005163, 2020.

Mathew, M. J., Menier, D., Siddiqui, N., Kumar, S. G., and Authemayou, C.: Active tectonic deformation along rejuvenated faults in tropical Borneo: Inferences obtained from tectono-geomorphic evaluation, Geomorphology, 267, 1–15, https://doi.org/10.1016/j.geomorph.2016.05.016, 2016.

545   Menier, D., Mathew, M., Pubellier, M., Sapin, F., Delcaillau, B., Siddiqui, N., Ramkumar, Mu., and Santosh, M.: Landscape response to progressive tectonic and climatic forcing in NW Borneo: Implications for geological and geomorphic controls on flood hazard, Sci Rep, 7, 457, https://doi.org/10.1038/s41598-017-00620-y, 2017.

Michetti, A.M., Esposito, E., Gurpinar, A., Mohammadioun, B., Mohammadioun, G., Porfido, S., Roghozin, E., Serva, L., Tatevossian, R., Vittori, E., Audemard, F., Comerci, V., Marco, S., Mccalpin, J. and Morner, N.A.: The INQUA Scale. An

550   innovative approach for assessing earthquake intensities based on seismically-induced ground effects in natural environment, In Memorie Descrittive della Carta Geologica d'Italia, Special Volume 67 (ed. Vittori E., and Comerci V.), (APAT, Rome 2004) pp. 1–118, 2004.

Michetti, A. M., Esposito, E., Guerrieri, L., Porfido, S., Serva, L., Tatevossian, R., ... and Roghozin, E.: Environmental seismic intensity scale-ESI 2007. Memorie descrittive della carta geologica d'Italia, 74, 41, 2007.

555   Mustafar, M. A., Simons, W. J. F., Tongkul, F., Satirapod, C., Omar, K. M., and Visser, P. N. A. M.: Quantifying deformation in North Borneo with GPS, J Geod, 91, 1241–1259, https://doi.org/10.1007/s00190-017-1024-z, 2017.

Nowicki Jessee, M. A., Hamburger, M. W., Allstadt, K., Wald, D. J., Robeson, S. M., Tanyas, H., Hearne, M., and Thompson, E. M.: A Global Empirical Model for Near-Real-Time Assessment of Seismically Induced Landslides, J. Geophys. Res. Earth Surf., 123, 1835–1859, https://doi.org/10.1029/2017JF004494, 2018.

560   Ota, Y., Azuma, T., and Lin, Y. N.: Application of INQUA Environmental Seismic Intensity Scale to recent earthquakes in Japan and Taiwan, Geological Society, London, Special Publications, 316, 55–71, https://doi.org/10.1144/SP316.4, 2009.

Papathanassiou, G., Valkaniotis, S., and Ganas, A.: Spatial patterns, controlling factors, and characteristics of landslides triggered by strike-slip faulting earthquakes: case study of Lefkada island, Greece, Bull Eng Geol Environ, 80, 3747–3765, https://doi.org/10.1007/s10064-021-02181-x, 2021.

565   Pescaroli, G. and Alexander, D.: Critical infrastructure, panarchies and the vulnerability paths of cascading disasters, Nat Hazards, 82, 175–192, https://doi.org/10.1007/s11069-016-2186-3, 2016.

Quigley, M. C., Attanayake, J., King, A. and Prideaux, F.: A multi-hazards earth science perspective on the COVID-19 pandemic: the potential for concurrent and cascading crises. Environment Systems and Decisions, 40(2), 199-215, 2020.

Rosli, M. I., Che Ros, F., Razak, K. A., Ambran, S., Kamaruddin, S. A., Nor Anuar, A., Marto, A., Tobita, T., and Ono, Y.: Modelling Debris Flow Runout: A Case Study on the Mesilau Watershed, Kundasang, Sabah, Water, 13, 2667, https://doi.org/10.3390/w13192667, 2021a.

Rosli, M. I., Mohd Kamal, N. A., and Razak, K. A.: Assessing Earthquake-induced Debris Flow Risk in the first UNESCO World Heritage in Malaysia, Remote Sensing Applications: Society and Environment, 23, 100550, https://doi.org/10.1016/j.rsase.2021.100550, 2021b.

Sapin, F., Hermawan, I, Pubellier, M., Vigny, C., and Ringenbach, J.-C.: The recent convergence on the NW Borneo Wedge—a crustal-scale gravity gliding evidenced from GPS, 193, 549–556, https://doi.org/10.1093/gji/ggt054, 2013.

Schmitt, R. G., Tanyas, H., Jessee, M. A. N., Zhu, J., Biegel, K. M., Allstadt, K. E., ... and Knudsen, K. L.: An open repository of earthquake-triggered ground-failure inventories (No. 1064). US Geological Survey, 2017.

Serva, L., Vittori, E., Comerci, V., Esposito, E., Guerrieri, L., Michetti, A. M., Mohammadioun, B., Mohammadioun, G. C., Porfido, S., and Tatevossian, R. E.: Earthquake Hazard and the Environmental Seismic Intensity (ESI) Scale, Pure Appl. Geophys., 173, 1479–1515, https://doi.org/10.1007/s00024-015-1177-8, 2016.

Shah, A., Zhafri, M., Delson, J., and Navakanesh, B.: Major Strike-Slip Faults Identified Using Satellite Data in Central Borneo, SE Asia, Geosciences, 8, 156, https://doi.org/10.3390/geosciences8050156, 2018.

Silva, P. G., Pérez-López, R., Rodríguez-Pascua, M. A., Giner, J. L., Huerta, P., Bardají, T. and Martín-González, F.: Earthquake environmental effects (EEEs) triggered by the 2011 Lorca earthquake (Mw 5.2, Betic Cordillera, SE Spain): Application of the ESI-07 macroseismic scale. 4th INQUA PATA meeting, Aachen, Germany, 2013.

Simons, W. J. F., Socquet, A., Vigny, C., Ambrosius, B. A. C., Haji Abu, S., Promthong, C., Subarya, C., Sarsito, D. A., Matheussen, S., Morgan, P., and Spakman, W.: A decade of GPS in Southeast Asia: Resolving Sundaland motion and boundaries, J. Geophys. Res., 112, B06420, https://doi.org/10.1029/2005JB003868, 2007.

Tanyaş, H., van Westen, C. J., Allstadt, K. E., Anna Nowicki Jessee, M., Görüm, T., Jibson, R. W., Godt, J. W., Sato, H. P., Schmitt, R. G., Marc, O., and Hovius, N.: Presentation and Analysis of a Worldwide Database of Earthquake-Induced Landslide Inventories: Earthquake-Induced Landslide Inventories, J. Geophys. Res. Earth Surf., 122, 1991–2015, https://doi.org/10.1002/2017JF004236, 2017.

Tanyaş, H., Görüm, T., Kirschbaum, D. and Lombardo, L.: Could road constructions be more hazardous than an earthquake in terms of mass movement?, Nat Haz, 1-25, 2022.

Tjia, H. D.: Kundasang (Sabah) at the intersection of regional fault zones of Quaternary age, BGSM, 53, 59–66, https://doi.org/10.7186/bgsm53200710, 2007.

Tongkul, F.: The 2015 Ranau Earthqauke: Cause and Impact. Sabah Society Journal, 32, 1-28, 2016.

Tongkul, F.: Active tectonics in Sabah—seismicity and active faults, BGSM, 64, 27–36, https://doi.org/10.7186/bgsm64201703, 2017.

Wang, Y., Wei, S., Wang, X., Lindsey, E. O., Tongkul, F., Tapponnier, P., Bradley, K., Chan, C.-H., Hill, E. M., and Sieh, K.: The 2015 M w 6.0 Mt. Kinabalu earthquake: an infrequent fault rupture within the Crocker fault system of East Malaysia, Geosci. Lett., 4, 6, https://doi.org/10.1186/s40562-017-0072-9, 2017.

Wang, F., Fan, X., Yunus, A. P., Siva Subramanian, S., Alonso-Rodriguez, A., Dai, L., Xu, Q., and Huang, R.: Coseismic landslides triggered by the 2018 Hokkaido, Japan (Mw 6.6), earthquake: spatial distribution, controlling factors, and possible failure mechanism, Landslides, 16, 1551–1566, https://doi.org/10.1007/s10346-019-01187-7, 2019.

Williams, J. G., Rosser, N. J., Kincey, M. E., Benjamin, J., Oven, K. J., Densmore, A. L., Milledge, D. G., Robinson, T. R., Jordan, C. A., and Dijkstra, T. A.: Satellite-based emergency mapping using optical imagery: experience and reflections from the 2015 Nepal earthquakes, Nat. Hazards Earth Syst. Sci., 18, 185–205, https://doi.org/10.5194/nhess-18-185-2018, 2018.

Xu, C.: Preparation of earthquake-triggered landslide inventory maps using remote sensing and GIS technologies: Principles and case studies, Geoscience Frontiers, 6, 825–836, https://doi.org/10.1016/j.gsf.2014.03.004, 2015.

Xu, C., Xu, X., Zhou, B., and Yu, G.: Revisions of the M 8.0 Wenchuan earthquake seismic intensity map based on co-seismic landslide abundance, Nat Hazards, 69, 1459–1476, https://doi.org/10.1007/s11069-013-0757-0, 2013.

Xu, C., Shyu, J. B. H., and Xu, X.: Landslides triggered by the 12 January 2010 Port-au-Prince, Haiti, Mw = 7.0 earthquake: visual interpretation, inventory compiling, and spatial distribution statistical analysis, Nat. Hazards Earth Syst. Sci., 14, 1789–1818, https://doi.org/10.5194/nhess-14-1789-2014, 2014.

Xu, C., Xu, X., Shen, L., Yao, Q., Tan, X., Kang, W., Ma, S., Wu, X., Cai, J., Gao, M., and Li, K.: Optimized volume models of earthquake-triggered landslides, Sci Rep, 6, 29797, https://doi.org/10.1038/srep29797, 2016.

Yusoff, H. H. M., Razak, K. A., Yuen, F., Harun, A., Talib, J., Mohamad, Z., Ramli, Z., and Razab, R. A.: Mapping of post-event earthquake induced landslides in Sg. Mesilou using LiDAR, IOP Conf. Ser.: Earth Environ. Sci., 37, 012068, https://doi.org/10.1088/1755-1315/37/1/012068, 2016.

Zuccaro, G., De Gregorio, D., and Leone, M. F.: Theoretical model for cascading effects analyses, International Journal of Disaster Risk Reduction, 30, 199–215, https://doi.org/10.1016/j.ijdrr.2018.04.019, 2018.